Emergence of Geometric Turing Patterns in Complex Networks

Jasper van der Kolk,[1,2,*] Guillermo García-Pérez,[3] Nikos E. Kouvaris,[4] M. Ángeles Serrano,[1,2,5,†] and Marián Boguñá[1,2,‡]

[1]*Departament de Física de la Matèria Condensada, Universitat de Barcelona, Martí i Franquès 1, E-08028 Barcelona, Spain*
[2]*Universitat de Barcelona Institute of Complex Systems (UBICS), Martí i Franquès 1, E-08028 Barcelona, Spain*
[3]*Algorithmiq Ltd, Kanavakatu 3C, FI-00160 Helsinki, Finland*
[4]*Dribia Data Research Sociedad Limitada, Carrer Llacuna 162, 08018 Barcelona, Spain*
[5]*Institució Catalana de Recerca i Estudis Avançats (ICREA), Passeig Lluís Companys 23, E-08010 Barcelona, Spain*

(Received 12 December 2022; revised 5 May 2023; accepted 22 May 2023; published 22 June 2023)

Turing patterns, arising from the interplay between competing species of diffusive particles, have long been an important concept for describing nonequilibrium self-organization in nature and have been extensively investigated in many chemical and biological systems. Historically, these patterns have been studied in extended systems and lattices. Recently, the Turing instability was found to produce topological patterns in networks with scale-free degree distributions and the small-world property, although with an apparent absence of geometric organization. While hints of explicitly geometric patterns in simple network models (e.g., Watts-Strogatz) have been found, the question of the exact nature and morphology of geometric Turing patterns in heterogeneous complex networks remained unresolved. In this work, we study the Turing instability in the framework of geometric random graph models, where the network topology is explained using an underlying geometric space. We demonstrate that not only can geometric patterns be observed, their wavelength can also be estimated by studying the eigenvectors of the annealed graph Laplacian. Finally, we show that Turing patterns can be found in geometric embeddings of real networks. These results indicate that there is a profound connection between the function of a network and its hidden geometry, even when the associated dynamical processes are exclusively determined by the network topology.

DOI: 10.1103/PhysRevX.13.021038

Subject Areas: Complex Systems, Interdisciplinary Physics, Nonlinear Dynamics

I. INTRODUCTION

In his 1952 seminal paper [1], Turing described how competing species of diffusive particles can cause a wide variety of patterns, starting from a spatially homogeneous state. Ever since, reaction-diffusion processes have been shown to host a wide variety of self-organizational behavior [2–9]. Historically, these behaviors have mostly been studied on regular lattices or in continuous media, but there has long been evidence for their existence also in systems of interconnected elements with complex structures. For instance, in the framework of embryonic morphogenesis, which was Turing's original motivation, it has been argued that embryos should be thought of as a multicellular network rather than a continuous medium [10]. However, complex network architecture makes the investigation of dynamical processes difficult, and studies have often been restricted to small networks [11–13].

In the context of network science, Nakao and Mikhailov made a step forward and demonstrated the existence of the Turing instability in systems of activator-inhibitor species diffusing in large random graphs [11]. In that work, the instability and the corresponding emerging patterns are intimately related to the degree heterogeneity usually present in real networks and are, thus, purely topological in nature.

Similar results have since been found for directed [14], non-normal [15], and temporal networks [16,17], as well as for networks with higher order interactions such as hypergraphs [18] and simplicial complexes [19]. Another example of nongeometric pattern formation in networks can be

*jasper.vanderkolk@ub.edu
†marian.serrano@ub.edu
‡marian.boguna@ub.edu

found in the context of multilayered networks, where particles diffuse not only within network layers but also between them [20–23]. Here, the dynamical parameters can be chosen such that the particle concentration within a layer is homogeneous whereas the distribution between layers is heterogeneous. Similar patterns can be found in networks displaying community structure [24], where concentrations can be chosen to be homogeneous within a community and heterogeneous between communities. It has been shown that these types of patterns can also be reproduced in empirical networks, provided their community structure is sufficiently strong.

While hints of explicitly geometric patterns in simple network models were found in several works [14,25–27], no comprehensive study of this phenomenon has been undertaken. Most importantly, the network models described in these studies are not suitable to describe real systems. In fact, geometric domains in a classical sense, typical of Turing patterns in lattices and continuous media, have not been observed in real complex networks. This is a consequence of the apparent lack of geometric structure in small-world networks, causing topological distances between nodes—measured by the shortest path lengths on the graph—to collapse around the average value, scaling logarithmically (or slower) with the system size.

This paradigm has changed recently with the development of network geometry [28]. Indeed, a latent metric space with hyperbolic geometry underlying real complex networks provides the simplest explanation to many of their observed topological properties, including heterogeneous degree distributions [29–31], clustering [30–34], small-worldness [35–37], and percolation [38,39], spectral [40], and self-similarity properties [29,41,42]. These models have been extended to growing networks [43], weighted networks [44], multilayer networks [45,46], networks with community structure [47–49], and they are also the basis for defining a renormalization group for complex networks [41,42].

In this paper, we show that the Turing instability triggers the emergence of purely geometric patterns that become evident in the latent space of real complex networks. We analyze this phenomenon within the framework of network geometry and find the relation between the parameters of the dynamical model and the general properties of the network, such as the congruency of the network with the underlying network space and the level of heterogeneity of its degree distribution.

II. BACKGROUND

The Turing instability arises as a consequence of the different diffusivity rates between activator and inhibitor species. Starting from a homogeneous concentration of particles, upon small perturbations, the system evolves towards a stable state with regions of high concentration of particles, coexisting with regions of low concentration. When the dynamics takes place on a metric space, these inhomogeneities give rise to geometric patterns. It is important to note that the first assumption of this framework is that diffusion alone, without the activation-inhibition mechanism, should lead to a homogeneous distribution of particles.

In continuous media, diffusion is modeled by Brownian particles and, in degree regular lattices, by standard random walks. Diffusion in complex networks is, however, different. Indeed, a simple random walk process on a heterogeneous network leads to a steady state where the concentration of particles is proportional to the degree of each node and, so, highly heterogeneous. Thus, before adding the activation-inhibition dynamics, we have to carefully define diffusion on networks to ensure that a homogeneous concentration of species is a fixed point of the dynamics. In Appendix A 1 we show that this can be achieved by a continuous time random walk with jump rates proportional to the current node's degree. Then, the evolution equation for the average concentration of particles at a given node i, $u_i(t)$, can be written as

$$\frac{du_i(t)}{dt} = -\epsilon \sum_{j=1}^{N} L_{ij} u_j(t), \tag{1}$$

where ϵ is the diffusion coefficient, N the number of nodes, and L_{ij} the Laplacian matrix defined as in Ref. [50]:

$$L_{ij} = k_j \delta_{ij} - a_{ij}. \tag{2}$$

In this last equation a_{ij} is the adjacency matrix of the network, that hereafter is assumed to describe a single connected component.

A. Activation-inhibition dynamics

In the diffusion process described by Eq. (1), particles do not interact when they meet in the same node. However, in realistic settings, particles may undergo all sorts of reaction processes. In particular, the Turing instability arises when two different species, U and V, interact upon meeting at the same node, under an activation-inhibition process. Within each node, species U undergoes an autocatalytic process and, simultaneously, favors the increase of the population of species V. At the same time, species V inhibits the growth of species U even though it cannot survive without it. When the average number of particles per node is large, we can neglect fluctuations in the number of particles and work under the mean field approximation. Let $u_i(t)$ and $v_i(t)$ be the average number of particles at node i of species U and V, respectively. Their evolution equations are given by

$$\frac{du_i(t)}{dt} = f[u_i(t), v_i(t)] - \epsilon \sum_{j=1}^{N} L_{ij} u_j(t), \tag{3}$$

$$\frac{dv_i(t)}{dt} = g[u_i(t), v_i(t)] - \sigma\epsilon \sum_{j=1}^{N} L_{ij} v_j(t), \tag{4}$$

where functions $f(u, v)$ and $g(u, v)$ represent the activation-inhibition dynamics within the nodes and ϵ and $\sigma\epsilon$ are the activator and inhibitor diffusion coefficients, respectively. We further assume that the system has a stable homogeneous stationary state, that is, $u_i^{\mathrm{st}} = \bar{u}$ and $v_i^{\mathrm{st}} = \bar{v}$, for which $f(\bar{u}, \bar{v}) = 0$ and $g(\bar{u}, \bar{v}) = 0$, so that $(\bar{u}, \bar{v})$ is a stable fixed point of the dynamics. The activation-inhibition dynamics and its stability condition impose constraints on functions $f(u, v)$ and $g(u, v)$. In particular, its first derivatives $f_u \equiv \partial_u f(\bar{u}, \bar{v})$, $f_v \equiv \partial_v f(\bar{u}, \bar{v})$, $g_u \equiv \partial_u g(\bar{u}, \bar{v})$, and $g_v \equiv \partial_v g(\bar{u}, \bar{v})$ must satisfy $f_u > 0$, $f_v < 0$, $g_u > 0$, $g_v < 0$, and $f_u + g_v < 0$, $f_u g_v - f_v g_u > 0$ (see Ref. [11] for further details).

The Turing instability arises when, due to the differences in the diffusion coefficients of the two species, the fixed point becomes unstable so that any small perturbation drives the system away from it. Interestingly, the conditions for this to take place depend only on f_u, f_v, g_u, g_v and the ratio between the diffusion coefficients of the two species σ. Similarly to the case of continuous media, where the perturbation around the fixed point can be expanded in Fourier modes—the eigenfunctions of the Laplacian ∇^2—and where the eigenvalues are related to the wave numbers, here the perturbation can be expanded in terms of the eigenvectors of the graph Laplacian L_{ij} [11],

$$u_i(t) - \bar{u} \approx \sum_{\alpha=1}^{N} c_\alpha e^{\lambda_\alpha t} \phi_i^\alpha, \tag{5}$$

where c_α and λ_α are some constants that depend on the parameters of the model Eqs. (3) and (4) and on the eigenvalue Λ_α (similarly for species V). This expansion is possible because the eigenvectors of the Laplacian matrix $\{\vec{\phi}^\alpha = (\phi_1^\alpha, \phi_2^\alpha, \ldots, \phi_N^\alpha); \alpha = 1, \ldots, N\}$ form a complete orthonormal basis of $\mathbb{R}^N$. If $\lambda_\alpha < 0$, $\forall\ \Lambda_\alpha$, then perturbations around the fixed point are absorbed exponentially fast, so that the fixed point is stable. However, if there exists at least one Λ_α such that $\lambda_\alpha > 0$, then the fixed point becomes unstable. In this case, those nodes with $c_\alpha \phi_i^\alpha > 0$ will increase the concentration of species U, whereas those with negative value will decrease it. Note that for all eigenvectors associated to nonvanishing eigenvalues we have

$$\sum_{i=1}^{N} \phi_i^\alpha = 0. \tag{6}$$

If we combine this with the fact that each component is associated to a given node of the network, we find that the dynamics will necessarily evolve toward a state with some of the nodes containing a high concentration of species U and the rest a low concentration.

In Ref. [11] it was shown that there exist unstable eigenvalues (i.e., $\lambda_\alpha > 0$) whenever

$$\sigma \geq \sigma_c = \frac{f_v g_u}{f_u^2} \left[\frac{f_u g_v}{f_v g_u} - 2 - 2\sqrt{1 - \frac{f_u g_v}{f_v g_u}} \right]. \tag{7}$$

In this regime, all eigenvalues that lie within the interval $\Lambda \in [\Lambda_-, \Lambda_+]$, with

$$\Lambda_\pm = \frac{1}{2\sigma\epsilon} \left[\sigma f_u + g_v \pm \sqrt{(\sigma f_u - g_v)^2 + 4\sigma f_v g_u} \right], \tag{8}$$

become unstable, with the most unstable one being

$$\Lambda_{\max} = \frac{1}{1-\sigma} \left[f_u - g_v - (1+\sigma)\sqrt{\frac{-f_v g_u}{\sigma}} \right]. \tag{9}$$

The functional dependence of Eqs. (7) and (8) implies that, for a given set of parameters f_u, f_v, g_u, g_v and for one particular eigenvalue Λ_α, it is always possible to select parameters ϵ and σ such that $\Lambda_\alpha \in [\Lambda_-, \Lambda_+]$. In the case that $\Lambda^+ \approx \Lambda^- \approx \Lambda_\alpha$, one can assume that the differences in the concentration of species in the nodes are encoded in the eigenvector $\vec{\phi}^\alpha$.

Interestingly, these results depend only on the first derivatives of functions $f(u, v)$ and $g(u, v)$ coupled to the diffusion coefficients. Therefore, there exists a whole class of systems where such instability may emerge, from chemical reactions [51–53] or biological morphogenesis [3,54] to ecosystems [55–58] and game theory applied to ecological systems [59,60]. In ecology, one such model is the Mimura-Murray model [56]. Here, u and v represent prey and predator densities, respectively, and the dynamics is governed by the functions

$$f(u, v) = \left[\frac{a + bu - u^2}{c} - v \right] u, \tag{10}$$

$$g(u, v) = [u - (1 + dv)]v. \tag{11}$$

From Eqs. (3), (4), (10), and (11), we see that in the absence of preys, predators go extinct and in the absence of predators, preys attain a constant population. In general, there is a fixed point with positive densities of preys and predators. In this paper, we use this dynamics as a case study (technical details are given in Appendix A 3).

B. Geometric description of complex networks: The $\mathbb{S}^1/\mathbb{H}^2$ model

As we have seen, the shape of emerging patterns is dictated by the arrangements of the signs in the components of the eigenvectors of the Laplacian matrix. In continuous media or regular lattices, these signs are arranged in the metric space in an alternating fashion, so that when the parameters of the dynamics are tuned to select these eigenvectors as unstable, the concentration of species also follows the same geometric pattern. In random graphs models, like the configuration model [61–64] or the Barábasi-Albert model [65], the situation is different. For these type of models, there is no associated metric space and the most distinctive feature of nodes is the degree. In this case, the Turing instability leads to patterns that are purely topological, with high or low concentration of species depending on nodes' degrees [11]. Real complex networks, however, are better described by geometric random graph models. In such models, nodes are embedded in a metric space and the connection probability depends on the distances among nodes in this metric space. This approach has led to the development of the field of network geometry [28], giving rise to the most comprehensive description of real complex networks.

To generate geometric networks, we use the $\mathbb{S}^1/\mathbb{H}^2$ model [29,30,66], otherwise known as the geometric soft configuration model [67]. The model combines a similarity dimension, encoded in a one-dimensional sphere, and a popularity dimension, quantified by nodes' degrees. In particular, each node is given a pair of hidden variables $\kappa_i \in [\kappa_0, \infty)$ and $\theta_i \in [0, 2\pi)$. The former accounts for the ith node's ensemble average degree, and can be generated from an arbitrary distribution $\rho(\kappa)$. The latter is the angular position of node i on the circle, as an abstraction of its position in the similarity space. In the simplest version of the model, κ and θ are statistically independent random variables and θ is homogeneously distributed. This final assumption, however, is not critical to our model and, in fact, in real systems the angular distribution is inhomogeneous, inducing the emergence of geometric communities [47–49,68,69]. The model is fully determined by the following connection probability between two nodes i and j:

$$p_{ij} = \frac{1}{1 + \left(\frac{x_{ij}}{\mu\kappa_i\kappa_j}\right)^{\beta}}, \tag{12}$$

where x_{ij} is the distance between the nodes in the circle of radius $R = N/2\pi$, $\beta > 1$ is the inverse of the temperature of the ensemble [30,34,67], and $\mu = (\beta/2\pi\langle k\rangle)\sin(\pi/\beta)$ a parameter fixing the average degree $\langle k\rangle$ of the network. While the model is defined for arbitrary distributions of hidden degrees, here we choose a power law distribution of the form $\rho(\kappa) = (\gamma-1)\kappa_0^{\gamma-1}\kappa^{-\gamma}$, with $\kappa \geq \kappa_0$. With this choice, the model becomes small-world whenever $1 < \beta \leq 2$, or $2 < \gamma \leq 3$, or both. Additionally, degree heterogeneity is modulated by the exponent γ and the limit $\gamma \to \infty$ is equivalent to a homogeneous distribution of hidden degrees $\rho(\kappa) = \delta(\kappa - \langle k\rangle)$ and a Poisson degree distribution.

As it is defined, the $\mathbb{S}^1$ model represents the only maximally random ensemble of geometric graphs that are simultaneously sparse, clustered, small-world, with heterogeneous degree distribution, and with only structural degree-degree correlations [67]. In the regime $\beta > 1$, the connection probability does not depend on the system size and, therefore, it generates networks with finite clustering in the thermodynamic limit. In this paper, we restrict ourselves to this regime of temperatures. However, the model has been extended to the case $\beta < 1$, showing interesting quasigeometric properties in the neighborhood of $\beta \lesssim 1$ even though clustering vanishes for $\beta \leq 1$ in the thermodynamic limit [34]. It is worth mentioning that the model is defined in arbitrary dimensions. However, as shown in Ref. [70], most real networks are well described by low dimensional spaces. Thus, to keep the analysis simple, we restrict ourselves to the one-dimensional case.

The $\mathbb{S}^1$ model is isomorphic to a purely geometric model in the hyperbolic plane of constant negative curvature -1, the so-called $\mathbb{H}^2$ [30] model. Upon mapping the hidden degree κ to a radial coordinate r as

$$r = R_{\mathbb{H}^2} - 2\,\ln\frac{\kappa}{\kappa_0}, \tag{13}$$

the connection probability Eq. (12) becomes

$$p_{ij} = \frac{1}{1 + e^{(\beta/2)(d_{\mathbb{H}^2,ij} - R_{\mathbb{H}^2})}}, \tag{14}$$

where $R_{\mathbb{H}^2} = 2\,\ln\,(N/\mu\pi\kappa_0^2)$ is the radius of a hyperbolic disk and $d_{\mathbb{H}^2,ij}$ is the hyperbolic distance between nodes i and j given by the hyperbolic law of cosines:

$$\cosh\,(d_{\mathbb{H}^2,ij}) = \cosh\,r_i\cosh\,r_j - \sinh\,r_i\sinh\,r_j\cos\,\Delta\theta_{ij}, \tag{15}$$

where $\Delta\theta_{ij}$ is the angular separation between the nodes. Because of this isomorphism, we are free to work with one version or the other indistinctly. In this paper, we use the $\mathbb{S}^1$ model to perform the analytical calculations and the $\mathbb{H}^2$ model for visualization.

III. MIMURA-MURRAY DYNAMICS ON GEOMETRIC NETWORKS

To illustrate the role of geometry on the Turing instability, we run the Mimura-Murray dynamics on a real network, namely that of the connectome of a mouse

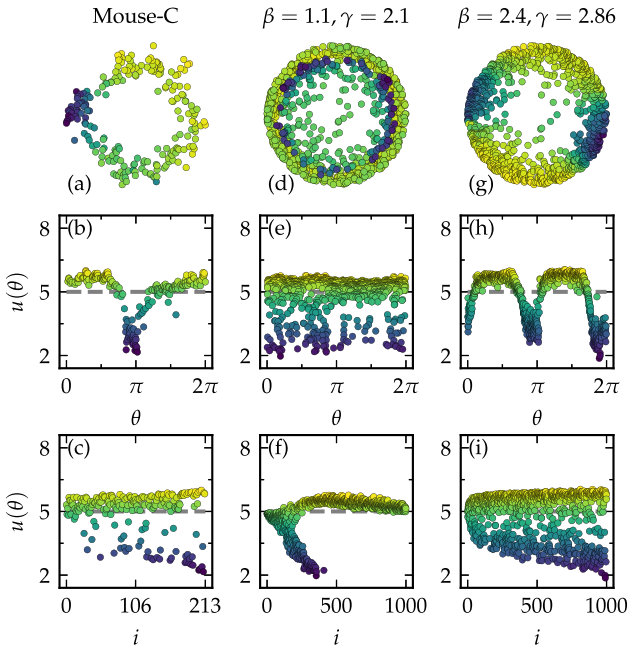

FIG. 1. Examples of Turing patterns in networks. The first, (a)–(c), is a real network representing the connectome of a mouse, the second, (d)–(f), a strongly heterogeneous $\mathbb{S}^1/\mathbb{H}^2$ network with parameters $(N, \langle k \rangle, \beta, \gamma) = (1000, 50, 1.1, 2.1)$, and the third, (g)–(i), a weakly heterogeneous $\mathbb{S}^1/\mathbb{H}^2$ network with parameters $(N, \langle k \rangle, \beta, \gamma) = (1000, 50, 2.4, 2.86)$. In all panels the colors correspond to the density of the activators in the final stationary state. In panels (a), (d), and (g) nodes are located according to their coordinates in hyperbolic space. Panels (b), (e), and (h) show the density of activators as a function of nodes' angular coordinates, and in panels (c), (f), and (i) the activators' densities are plotted against nodes' degree ranking.

described in Appendix A 5. Figure 1(a) shows the results on the concentration of species U in the hyperbolic representation of the network (see Sec. V for technical details). As can be seen, there is a clear pattern associated to the geometric organization of the network, with low concentrations of particles localized in the same angular position and high concentrations in the rest of the network. In Figs. 1(b) and 1(c), we also represent the concentration as a function of the angular coordinate θ and the node index i, respectively. In the latter case the nodes are ordered from high to low degree. It is important to note that the Mimura-Murray dynamics does not use any information from the underlying metric space, so that the observed geometric pattern is a highly nontrivial result.

To shed light on this problem, we also run the dynamics on networks generated by the $\mathbb{S}^1/\mathbb{H}^2$ model with a heterogeneous degree distribution with exponent γ. Figures 1(d)–1(i) show results of the dynamics on two different networks: one highly heterogeneous ($\gamma = 2.1$) and weakly clustered and a second one less heterogeneous ($\gamma = 2.84$) and highly clustered. In the strongly heterogeneous network shown in the figure, there are no patterns associated to the geometric character of the network. We do observe, however, topological patterns induced by degree, with high degree nodes holding a low concentration of species U. These are the type of patterns documented in Ref. [11]. Instead, in the case of the less heterogeneous network, we find a clear geometric pattern associated to the angular coordinates of nodes and very weak degree-related patterns, similar to the results found in the real network. These patterns emerge despite the fact that networks have the small-world property, so that diffusion induces flows of species between nodes that are far apart in the underlying metric space. These results suggest that some eigenvectors of the Laplacian of the $\mathbb{S}^1/\mathbb{H}^2$ model have a well-defined periodic structure in the similarity space. Next, we develop a theoretical framework allowing us to calculate an approximation for the frequency associated with such eigenvectors.

A. Eigenvectors of the $\mathbb{S}^1/\mathbb{H}^2$ Laplacian matrix in the annealed approximation

The goal of this section is to determine the dispersion relation $\omega(\Lambda)$ between the eigenvalue Λ and the frequency of its associated eigenvector. It needs to be stressed that this is a structural property of the network, and is not conditioned by the dynamics on top of the network.

Let us first note some important properties of the Laplacian matrix [50]. The Laplacian is a real symmetric matrix with real eigenvalues $\Lambda_1 = 0 \leq \Lambda_2 \leq \cdots \leq \Lambda_N \leq 2k_c$, where k_c is the maximum degree of the network. The average of all eigenvalues is equal to the network average degree, that is,

$$\langle \Lambda \rangle = \langle k \rangle, \tag{16}$$

and the second moment is

$$\langle \Lambda^2 \rangle = \langle k^2 \rangle + \langle k \rangle. \tag{17}$$

These results suggest that eigenvalues are strongly correlated to the sequence of degrees in the network. Additionally, as we show in Appendix A 4, in geometric random graph models, bounds on the isoperimetric (or Cheeger) constant [71,72] imply that the smallest non-null eigenvalue—the spectral gap—of the Laplacian approaches zero in the thermodynamic limit. In this limit, the spectrum is necessarily continuous on the positive real line as long as the node density along the circle and the connection probability are continuous functions and the degree distribution is unbounded. These facts imply that any eigenvector frequency given by $\omega(\Lambda)$ can be accessed by the system, as any real positive number will necessarily be arbitrarily close to an eigenvalue of the graph Laplacian for sufficiently large networks.

Species whose dynamics are governed by the Mimura-Murray model diffuse within a network with a disordered but quenched structure, a single realization of

the network ensemble defined by the $\mathbb{S}^1/\mathbb{H}^2$ model for a given sequence of hidden variables (κ_i, θ_i), $i = 1, \ldots, N$. Unfortunately, for quenched networks it is not possible to get any analytical insight on the structure of the eigenvectors of the Laplacian matrix. To overcome this problem, we use the annealed approximation, which has been extensively used in the literature to tackle a wide variety of problems, from neural networks and opinion dynamics to epidemic spreading [73–81]. In this approach, the network structure is resampled from the ensemble at a rate faster than the diffusion dynamics. This allows us to replace the adjacency matrix a_{ij} by its ensemble average, the connection probability p_{ij}, and consider the network not as a quenched system but as a dynamic one. With this approximation, the eigenvalue problem of the annealed Laplacian matrix can be written as

$$\sum_{j\neq i} \frac{\phi(\kappa_j,\theta_j)}{1+\left(\frac{x_{ij}}{\mu\kappa_i\kappa_j}\right)^\beta} = \left[\sum_{j\neq i} \frac{1}{1+\left(\frac{x_{ij}}{\mu\kappa_i\kappa_j}\right)^\beta} - \Lambda\right]\phi(\kappa_i,\theta_i), \quad (18)$$

where Λ is the eigenvalue and $\phi(\kappa_i, \theta_i)$ the component of the corresponding eigenvector of a node i with hidden variables (κ_i, θ_i). Note that, as in the case of the true Laplacian matrix, $\Lambda = 0$ is an eigenvalue with constant eigenvector.

In the thermodynamic limit, the curvature of the circle goes to zero and, thus, nodes become distributed in $\mathbb{R}^1$ according to a Poisson point process of density one. In this limit, the distance between two nodes can be evaluated as $x_{ij} = |x_i - x_j|$, where x_i and x_j are the positions of nodes i and j in $\mathbb{R}^1$. Finally, we take the continuum limit in Eq. (18) by replacing the sum over index j by a double integral over nodes coordinates (κ, x). In this way, Eq. (18) can be written as the following integral equation:

$$\int_{\kappa_0}^{\infty} \rho(\kappa')d\kappa' \int_{-\infty}^{\infty} dx' \frac{\phi(\kappa',x')}{1+\left(\frac{|x-x'|}{\mu\kappa\kappa'}\right)^\beta} = (\kappa-\Lambda)\phi(\kappa,x). \quad (19)$$

The spatial part of Eq. (19) has the form of a convolution integral. Thus, we can take advantage of the convolution theorem for Fourier transforms. By defining the Fourier transform of the eigenvector as

$$\hat{\phi}(\kappa,\omega) \equiv \int_{-\infty}^{\infty} e^{-i\omega x}\phi(\kappa,x)dx, \quad (20)$$

Eq. (19) can be written in Fourier space as

$$\int_{\kappa_0}^{\infty} \frac{\kappa'\rho(\kappa')}{\langle k\rangle} \frac{\hat{\Psi}(\mu\kappa\kappa'\omega)}{\hat{\Psi}(0)} \hat{\phi}(\kappa',\omega)d\kappa' = \frac{\kappa-\Lambda}{\kappa}\hat{\phi}(\kappa,\omega), \quad (21)$$

where we define $\hat{\Psi}$ as

$$\hat{\Psi}(z) \equiv \mathcal{F}\left[\frac{1}{1+|x|^\beta}\right](z), \quad (22)$$

where $\mathcal{F}$ stands for Fourier transform. Note that $\mu^{-1} = \langle k\rangle\hat{\Psi}(0)$. From Eq. (21), it is easy to see that the integral over the spatial coordinate of nontrivial eigenvectors must vanish, that is, $\hat{\phi}(\kappa, 0) = 0$, similarly to the case of the quenched Laplacian matrix Eq. (6). Indeed, by setting $\omega = 0$ in Eq. (21), we conclude that $\hat{\phi}(\kappa, 0) = 0$ is the only solution when $\Lambda \neq 0$. Thus, the annealed approximation preserves the basic property of the Laplacian matrix given in Eq. (6).

B. Homogeneous ensemble

The analytic solution of Eq. (21) can be found in particular cases. One such case is a homogeneous ensemble where all nodes have the same hidden degree, that is, $\rho(\kappa) = \delta(\kappa - \langle k\rangle)$, leading to a Poisson degree distribution of average $\langle k\rangle$. In this situation, the eigenvector is just a function of the frequency ω and Eq. (21) becomes

$$\left[\frac{\hat{\Psi}(\mu\langle k\rangle^2\omega)}{\hat{\Psi}(0)} - \frac{\langle k\rangle-\Lambda}{\langle k\rangle}\right]\hat{\phi}(\omega) = 0. \quad (23)$$

Assuming that $\hat{\phi}(\omega) \neq 0$, this equation defines a dispersion relation between the eigenvalue Λ and its characteristic frequency ω_c as a solution of the transcendent equation:

$$\frac{\Lambda(\omega_c)}{\langle k\rangle} = \left[1 - \frac{\hat{\Psi}(\mu\langle k\rangle^2\omega_c)}{\hat{\Psi}(0)}\right]. \quad (24)$$

The characteristic frequency ω_c in Eq. (24) is constrained by the boundary conditions and the discretization of nodes in the space. Indeed, since nodes are distributed on the line at density 1, frequencies above π (and so wavelengths of the order 1) cannot be detected. Additionally, if the system is finite of length $L = N$, frequencies below $2\pi/N$ will have associated wavelengths comparable to the system size and, so, will not be detected either. Therefore, we look for solutions of Eq. (24) in the domain $\omega_c \in [2\pi/N, \pi]$.

It is illustrative to analyze in detail the homogeneous case with $\beta = \infty$, which corresponds to a connection probability being a step function. In this case, function $\hat{\Psi}(z)$ takes the form

$$\hat{\Psi}(z) = 2\frac{\sin z}{z}, \quad (25)$$

and $\mu = 1/(2\langle k\rangle)$. Combining these results, the dispersion relation defining ω_c becomes

$$\frac{\Lambda(\omega_c)}{\langle k\rangle} = \left(1 - \frac{2\sin\frac{\langle k\rangle\omega_c}{2}}{\langle k\rangle\omega_c}\right). \quad (26)$$

In the case of $\beta = \infty$, nodes connect to nearest neighbors on the line that are below a certain critical distance, so that the average number of such neighbors is $\langle k\rangle$. Therefore,

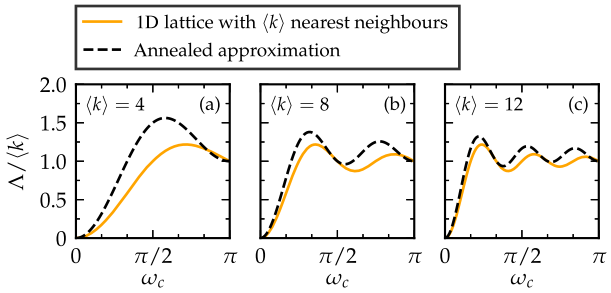

FIG. 2. Dispersion relation for the annealed approximation and a degree-regular one-dimensional lattice. Solid orange lines show exact results from Eq. (27) and black dashed lines for the annealed approximation in Eq. (26) for homogeneous networks with $\beta = \infty$. Results are shown for average degrees $\langle k \rangle = 4$, 8, and 12.

apart from the fluctuations in the number of neighbors, the dispersion relation in Eq. (26) should be equivalent to the dispersion relation of a one-dimensional lattice with $\langle k \rangle$ symmetric nearest neighbors, which reads

$$\frac{\Lambda}{\langle k \rangle} = 1 - \frac{2}{\langle k \rangle} \sum_{n=1}^{\langle k \rangle/2} \cos\, n\omega_c. \tag{27}$$

Figure 2 shows the comparison between Eqs. (26) and (27) for $\langle k \rangle = 4$, 8, and 12. Both expressions are very similar and become identical as the connectivity increases, in agreement with the fact that the continuum approximation becomes exact at infinite average degree.

Despite the good agreement shown in Fig. 2, the comparison with quenched networks generated by the $\mathbb{S}^1/\mathbb{H}^2$ model has to be made with care. Indeed, for homogeneous networks, the annealed approximation completely neglects fluctuations of nodes' degrees. In a quenched network this is far from true, as the degree distribution follows a Poisson distribution of average $\langle k \rangle$. However, the dispersion relations Eqs. (26) and (27) are strongly dependent on the network connectivity, especially in the high frequency domain. Therefore, due to the randomness of nodes' degrees, it is not possible to characterize each eigenvector of the quenched Laplacian by a unique frequency but by a collection of frequencies around a given average.

We cannot talk then of a deterministic dispersion relation but a fuzzy one where different frequencies may coexist in the same eigenvector. This will destroy any possible high frequency periodic pattern, leaving only low frequency eigenvectors (with $\Lambda \ll \langle k \rangle$) visible. The reason is that low frequency modes correspond to long wavelengths, so that local fluctuations of degrees become irrelevant. This is clearly visible in Figs. 3(a)–3(c), showing three different eigenvectors of the annealed Laplacian

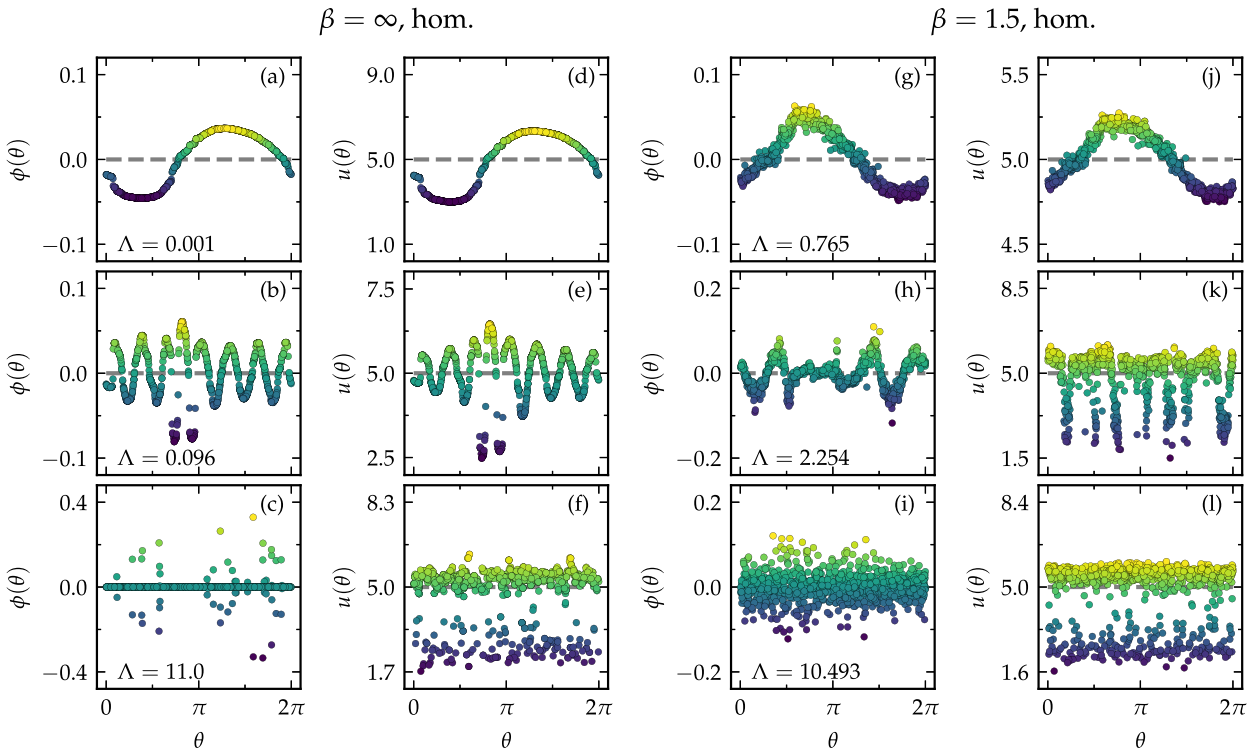

FIG. 3. (a)–(c),(g)–(i) Examples of three eigenvectors of the quenched Laplacian matrix with low, medium, and high associated frequencies for a single network generated by the homogeneous ensemble with $N = 1000$ and $\langle k \rangle = 20$ and $\beta = \infty$ (a)–(c) and $\beta = 1.5$ (g)–(i). (d)–(f),(j)–(l) Concentration of species U in the Mimura-Murray dynamics for the eigenvalues in the column to the left of each panel.

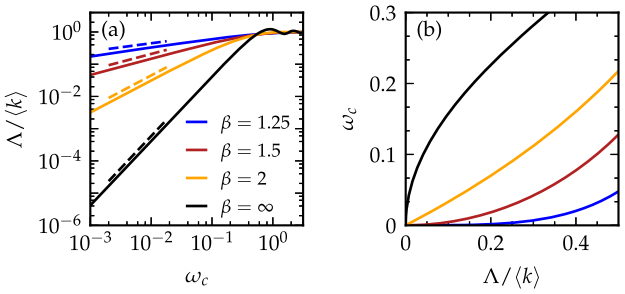

FIG. 4. (a) Rescaled eigenvalue as a function of the characteristic frequency in log-log scale. (b) Characteristic frequency as a function of the rescaled eigenvalue. In both cases $\langle k\rangle = 10$ and several β's are investigated.

matrix corresponding to low, medium, and high frequencies of a graph generated by the homogeneous ensemble. The periodic pattern is very clear in the case of low eigenvalue with very low frequency. In the medium frequency case, we can still identify a periodic behavior, although distorted by noise. In the case of high frequency, periodic behavior is totally absent. We also run the Mimura-Murray dynamics on the same network selecting parameters' values such that the same eigenvalues used in Figs. 3(a)–3(c) become unstable (see Appendix A 3 for technical details of the dynamics). Figures 3(d)–3(f) show the concentration of species U in the three cases. We observe that the patterns in the concentration of species U closely follow the patterns of the corresponding eigenvectors, justifying the relevance of the structure of eigenvectors for dynamical processes on networks.

Based on these observations, we conclude that the annealed approximation provides good results in quenched networks for small eigenvalues such that $\Lambda \ll \langle k\rangle$, which corresponds to low frequencies, that is, $\mu\langle k\rangle^2\omega_c \ll 1$. For arbitrary values of β, we can then take the low frequency limit in Eq. (24) to derive the relation between ω_c and Λ. Using the definition of the Fourier transform, it is easy to see that for small z,

$$1 - \frac{\hat{\Psi}(z)}{\hat{\Psi}(0)} \sim \begin{cases} z^{\beta-1} & \beta \leq 3 \\ z^2 & \beta > 3. \end{cases} \tag{28}$$

Figure 4(a) shows the low frequency limit of the dispersion relation computed numerically for different values of β, which corroborates this scaling behavior. Using this result, the characteristic frequency scales as

$$\omega_c \sim \begin{cases} \dfrac{1}{\langle k\rangle}\left(\dfrac{\Lambda}{\langle k\rangle}\right)^{1/(\beta-1)} & \beta \leq 3 \\ \dfrac{1}{\langle k\rangle}\sqrt{\dfrac{\Lambda}{\langle k\rangle}} & \beta > 3. \end{cases} \tag{29}$$

The fact that $(\beta-1)^{-1} < 1/2$ implies that, in this regime, a certain eigenvalue leads to a much lower frequency in the case of small β's than it does for high β's, an observation that is corroborated by Fig. 4(b).

Figures 3(g)–3(l) show the same analysis as in Figs. 3(a)–3(f) but for the case $\beta = 1.5$, so that networks are deep into the small-world regime, with many long-range connections among distant nodes in the metric space. We observe the same qualitative behavior as in the case $\beta = \infty$, except that, as expected, results have more noise. Yet, we can clearly identify geometric patterns both in the eigenvectors and in the steady state of the Mimura-Murray dynamics when the dynamic parameters are properly tuned. However, we notice that, in agreement with our theoretical prediction in Eq. (29), eigenvalues with similar associated eigenvector frequencies as those in Figs. 3(a) and 3(d) are significantly larger.

C. Heterogeneous ensemble

In real networks, the degree distribution is typically heterogeneous. Therefore, we have to solve the eigenvalue problem in Eq. (21) for a heterogeneous distribution of hidden degrees $\rho(\kappa)$. In particular, we choose a scale-free distribution $\rho(\kappa) \propto \kappa^{-\gamma}$. For this distribution of hidden degrees, Eq. (21) can be rewritten as

$$(\gamma-2)\int_0^1 \frac{z'^{\gamma-3}}{1-\tilde{\Lambda}z'}\hat{\Omega}\left(\frac{\tilde{\omega}}{zz'}\right)\hat{\Theta}(z',\tilde{\omega})dz' = \hat{\Theta}(z,\tilde{\omega}), \tag{30}$$

where we redefine variables $(\kappa, \Lambda, \omega)$ as

$$z \equiv \frac{\kappa_0}{\kappa}, \qquad \tilde{\Lambda} \equiv \frac{\Lambda}{\kappa_0}, \qquad \tilde{\omega} \equiv \mu\kappa_0^2\omega, \tag{31}$$

and functions as

$$\hat{\Omega}(x) \equiv \frac{\hat{\Psi}(x)}{\hat{\Psi}(0)}, \quad \hat{\Theta}(z,\tilde{\omega}) \equiv (1-\tilde{\Lambda}z)\hat{\phi}\left(\frac{\kappa_0}{z}, \frac{\tilde{\omega}}{\mu\kappa_0^2}\right). \tag{32}$$

When $\tilde{\Lambda} < 1$, the singularity of the kernel in the integral of Eq. (30) falls outside the domain of integration. In this case, Eq. (30) can be solved numerically by Gaussian quadrature as the solution of the system of equations,

$$\sum_{j=1}^{n}(\gamma-2)\frac{w_j z_j^{\gamma-3}}{1-\tilde{\Lambda}z_j}\hat{\Omega}\left(\frac{\tilde{\omega}}{z_i z_j}\right)\hat{\Theta}(z_j,\tilde{\omega}) = \hat{\Theta}(z_i,\tilde{\omega}), \tag{33}$$

where z_i, with $i = 1, \ldots, n$, are the zeros of the orthogonal polynomials used in the quadrature, w_i their associated weights, and $n \gg 1$ the number of points within the domain of integration used to evaluate the integral.

Equation (33) defines a homogeneous system of linear equations with kernel matrix $\mathbb{K}(\Lambda,\omega)$ given by

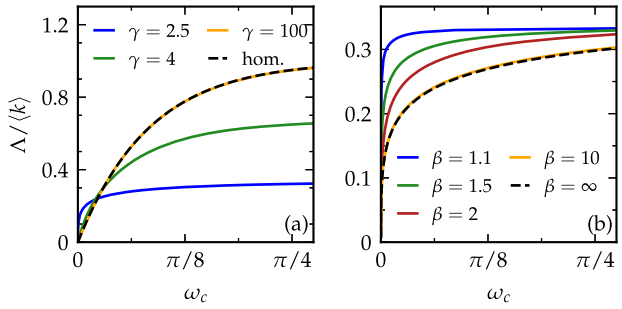

FIG. 5. (a) Dispersion relation obtained with Gaussian quadrature for $\beta = 2$ for various γ's and (b) the dispersion relation for $\gamma = 2.5$ and varying β. The average degree is $\langle k\rangle = 12$ in both panels.

$$K_{ij} \equiv (\gamma - 2)\frac{w_j z_j^{\gamma-3}}{1 - \tilde{\Lambda} z_j}\hat{\Omega}\left(\frac{\tilde{\omega}}{z_i z_j}\right) - \delta_{ij}. \tag{34}$$

A nonzero solution is found when $\det[\mathbb{K}(\Lambda, \omega)] = 0$, defining thus the dispersion relation $\Lambda(\omega_c)$. We use this condition to compute numerically the dispersion relation for different values of β and γ. Figure 5(a) shows the results for $\beta = 2$ and different values of γ and Fig. 5(b) shows the results for $\gamma = 2.5$ and different values of β. The dispersion relations are qualitatively similar to the homogeneous case with $\beta \leq 2$. The main difference appears in the asymptotic behavior of $\Lambda(\omega_c)$, which approaches κ_0 at high frequencies. Given the relation between the average degree and κ_0, this result implies that the ratio $\Lambda/\langle k\rangle$ approaches $(\gamma - 2)/(\gamma - 1)$, a value that is below 1. Therefore, the condition $\langle\Lambda\rangle = \langle k\rangle$ implies that the number of eigenvalues with periodic behavior can only account for a small fraction of all eigenvalues, and this fraction vanishes when $\gamma \approx 2$, as shown in Fig. S1 of Supplemental Material [82]. We conjecture that the remaining eigenvalues, with $\Lambda > \kappa_0$, are those which cannot be characterized by a single frequency.

Figure 6 shows the same analysis performed in Fig. 3 but for heterogeneous networks with $\gamma = 2.5$ and $\beta = 2.5$. The low frequency eigenvector is clearly periodic, although we observe some deviations corresponding to low degree nodes. By increasing the eigenvalue, the periodicity is still preserved although the sinusoidal behavior is strongly modified. Finally, periodicity is destroyed at high eigenvalues. This behavior is, again, translated into the steady state of the Mimura-Murray dynamics so that, even in the presence of strong heterogeneity in the degree distribution, we are able to find geometric Turing patterns in the dynamics.

IV. NUMERICAL RESULTS ON SYNTHETIC $\mathbb{S}^1/\mathbb{H}^2$ NETWORKS

To confirm numerically our theoretical predictions for the dispersion relations, we need a systematic way of

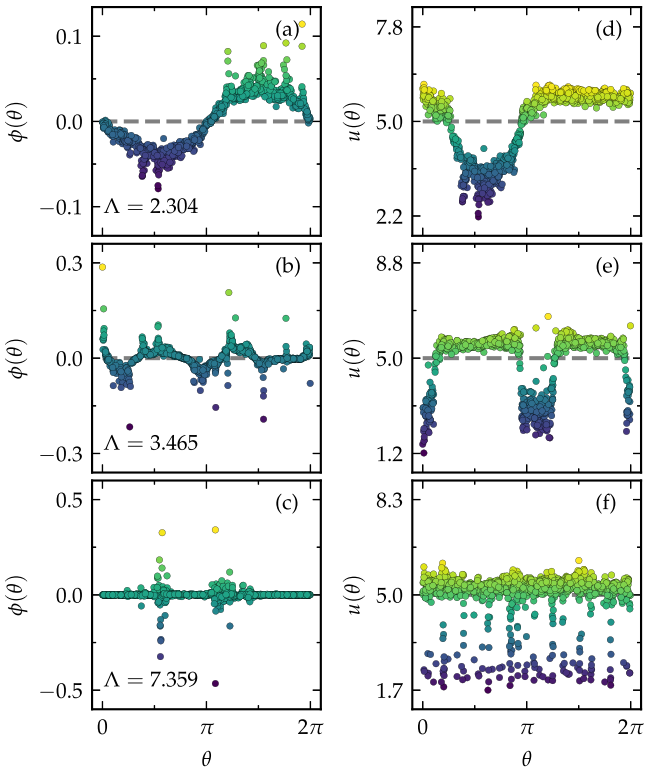

FIG. 6. (a)–(c) Examples of three eigenvectors with low, medium, and high associated frequencies for a single network generated by the heterogeneous ensemble with $N = 1000$, $\beta = 2.5$, $\gamma = 2.5$, and $\langle k\rangle = 20$. (d)–(f) Concentration of species U in the Mimura-Murray dynamics for the eigenvalues of the left-hand column.

determining when an eigenvector is periodic and, if so, what its dominant frequency is. To do so, we perform a discrete Fourier transform (DFT) on the eigenvectors and apply a statistical p-value test with the null hypothesis being that the Fourier signal is the result of white noise (see Appendix A 2 for further details). We apply this procedure to all eigenvalues and select those with statistically significant periodic signals. For each set of parameters β and γ, we repeat this procedure for a large number of network realizations and average the values of Λ obtained corresponding to a given frequency.

The result of this program is shown in Figs. 7(a)–7(d) for the homogeneous ensemble with $\beta = \infty$ and $\beta = 1.5$, and in Figs. 7(e)–7(h) for the heterogeneous ensemble with $\gamma = 2.5$ and $\beta = \infty$ and $\beta = 1.5$. As can be seen, the agreement with the annealed approximation is very good in all cases, with small deviations in the case of $\beta = 1.5$. These are understandable because networks generated by the $\mathbb{S}^1/\mathbb{H}^2$ model lose their metric character when β approaches one (as clustering goes to zero). Additionally, as mentioned in our previous discussion, it is not possible to find periodic behavior at high frequencies as the fluctuations of node degrees induce incoherent signals in the eigenvector structures. In the examples shown in Fig. 7, the null model

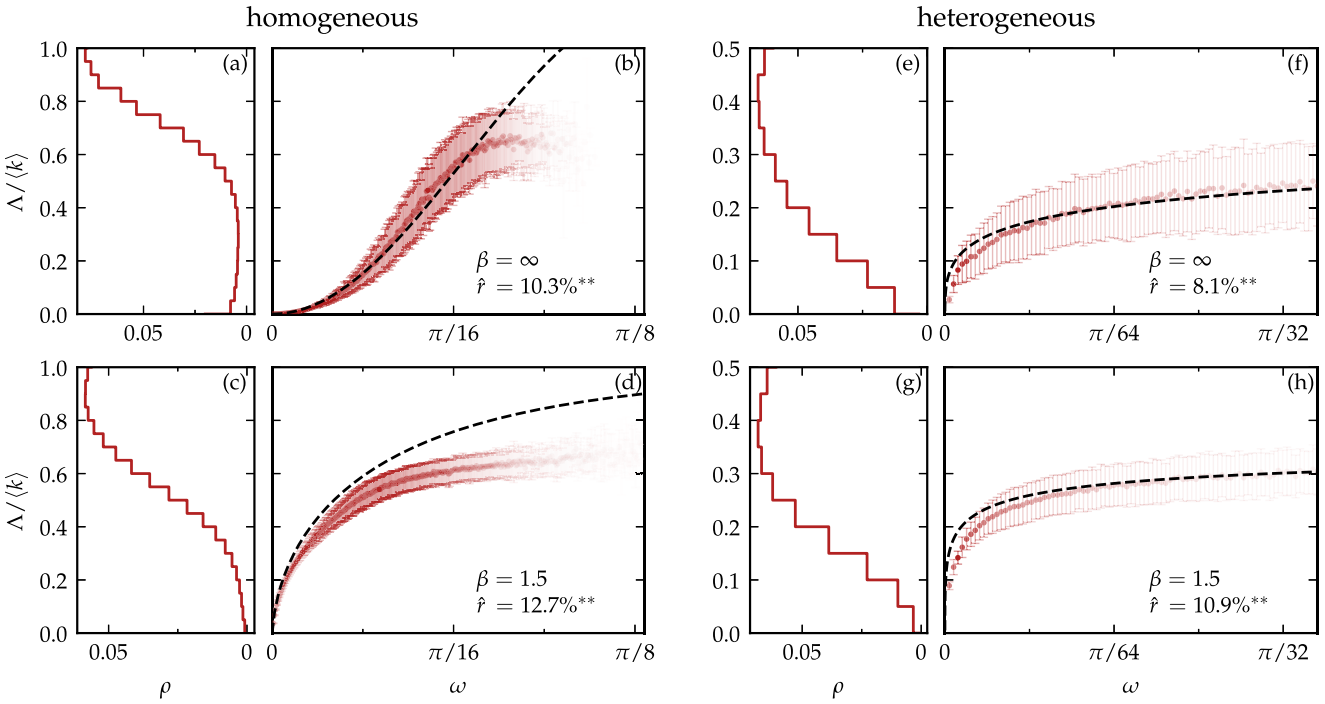

FIG. 7. (a),(c),(e),(g) Spectrum of an ensemble of networks generated by the homogeneous (a),(c) and heterogeneous (e),(g) ensembles with $\beta = 1.5$ (a),(e) and $\beta = 1.5$ (c),(g). For the heterogeneous ensemble $\gamma = 2.5$ is used. In all cases the average degree is given by $\langle k\rangle = 12$. (b),(d),(f),(h) Dispersion relation obtained by applying the fast Fourier transform to the eigenvectors and detecting the frequency with highest contribution. The opacity of the points is proportional to total amount of eigenvectors with the frequency corresponding to the point. The more transparent a point is, the fewer eigenvectors have that frequency. The black dashed lines are the theoretical predictions given by the annealed approximation. The parameter $\hat{r}$ gives the percentage of eigenvectors classified as periodic by the procedure described in Appendix A 2. The notation ** implies that the results are significant with $p = 0.01$.

combined with the DFT—using a confidence level of 2σ—is able to detect only between 8% and 12% of periodic eigenvalues.

V. REAL NETWORKS

To analyze the emergence of Turing patterns in real networks, we first need to find an embedding of the network under study in the hyperbolic plane. This amounts to finding, for each node of the network, its hidden degree κ and angular coordinate θ. For this task, we use Mercator [83], a tool which combines machine learning and maximum likelihood methods to find optimal embeddings congruent with the $\mathbb{S}^1/\mathbb{H}^2$ model. We then run the Mimura-Murray dynamics on the network and look for geometric patterns in the angular similarity space inferred by Mercator.

Of course, in the case of real networks, we expect less clean results as compared to synthetic graphs generated by the $\mathbb{S}^1/\mathbb{H}^2$ model. Indeed, there are four main factors affecting the emergence of Turing patterns in real networks. First, the embedding method is noisy, so that periodic patterns will also be noisy. Second, even if the embedding is perfect, the degree distribution is generally heterogeneous so that, as in the $\mathbb{S}^1/\mathbb{H}^2$ model, the range of observable frequencies is small. Third, as shown in Ref. [70], some real networks may be better represented in similarity spaces with dimension higher than $D = 1$. Thus, a geometric pattern in a high dimensional space can be distorted in a lower dimensional projection, making its detection difficult. Finally, the angular distribution in real networks is not perfectly uniform, with significant fluctuations defining geometric communities. As shown in Ref. [24], these communities have an impact on the eigenvector structure of the Laplacian matrix, so that in this case we should expect patterns with mixed effects from both the geometry of the network and its community structure. Despite all these limitations, we expect to find patterns in real networks associated to small nonvanishing eigenvalues.

Figure 8 shows results for four different real networks from different domains. Detailed definitions of these networks as well as those of several others which are analyzed in Supplemental Material [82] can be found in Appendix A 5. Figures 8(a)–8(d) show the structure of the eigenvector corresponding to a small eigenvalue (and lower frequency) for the four studied networks. The geometric patterns in the similarity space found by Mercator are very clear, with a wavelength of the order of the system size. The same structure is translated into

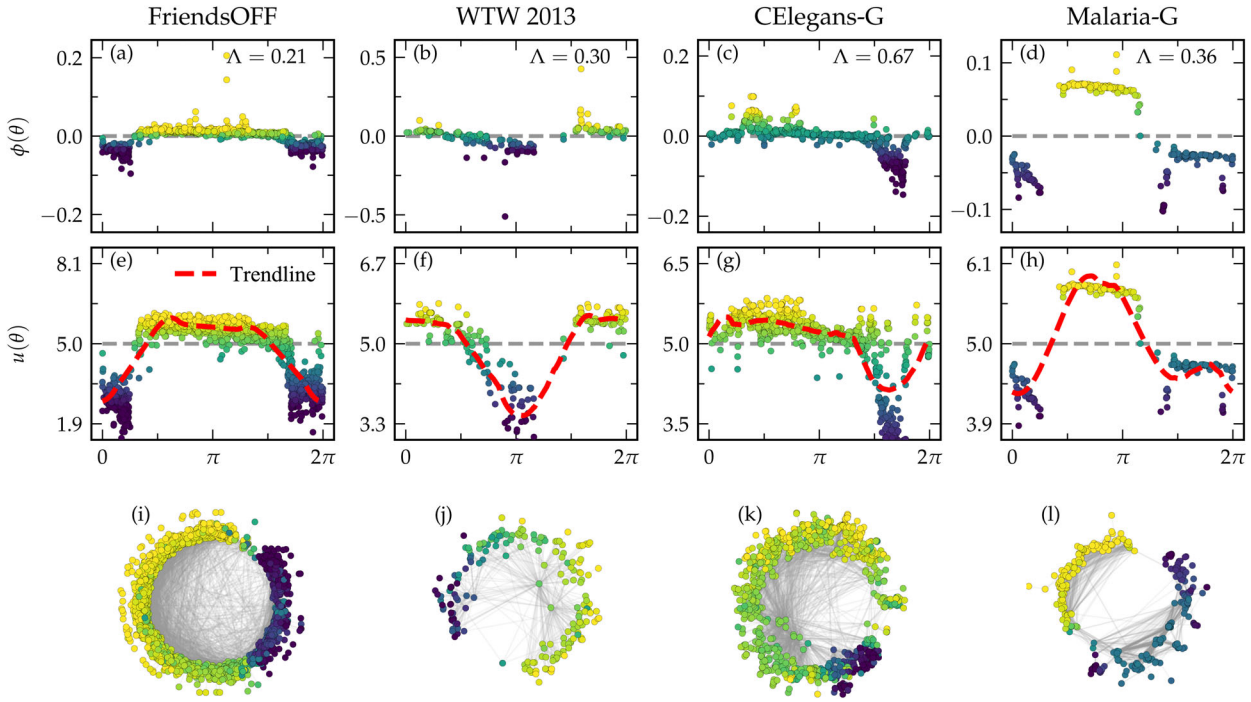

FIG. 8. (a)–(d) Eigenvectors $\phi(\theta)$ corresponding to the eigenvalue Λ as denoted in the figure for the real networks analyzed in this study, namely, FriendsOFF, an off-line friendship network; WTW 2013, the World-Trade-Web; CElegans-G, a network of genetic interaction of the nematode *C. elegans*; and Malaria-G, a network of highly variable genes of the human malaria parasite. (e)–(h) Concentration of species U for the Mimura-Murray dynamics setting the parameters to make these eigenvalues unstable. The red dotted line represents the trend obtained using the Savitzky-Golay filter with window size π. Panels (i)–(l) show the same as (e)–(h) but in the hyperbolic representation of the four networks.

the dynamics, as shown in Figs. 8(e)–8(h), where the same pattern can be recognized. We also plot a trendline, obtained by applying the Savitzky-Golay filter to the original signal. Finally, Figs. 8(i)–8(l) show the concentration of species U in the hyperbolic representation of the different networks inferred by Mercator. It is worth stressing how highly nontrivial this result is. Indeed, the Mimura-Murray dynamics generates steady states with correlation lengths of the order of the system size N in small-world networks where any pair of nodes is separated by a very small number of intermediate steps, scaling as $\ln N$. Additionally, this is achieved despite the fact that neither Mercator nor the Mimura-Murray dynamics use geometric information from the latent space as they take only the bare network topology as input.

Finally, we analyze in detail a human connectome network from Ref. [84] (see Appendix A 5 for details). This is an interesting example for which a significant number of patterns of different wavelengths can be detected. Figure 9(a) shows the dispersion relation between eigenvalues showing significant periodic signals versus their wave number. Despite the caveats discussed earlier, the dispersion relation agrees qualitatively well with the ones from the $\mathbb{S}^1$ model. In Figs. 9(c)–9(f) we show two of these patterns, corresponding to wave numbers one and two, where the patterns are clearly visible. Although the

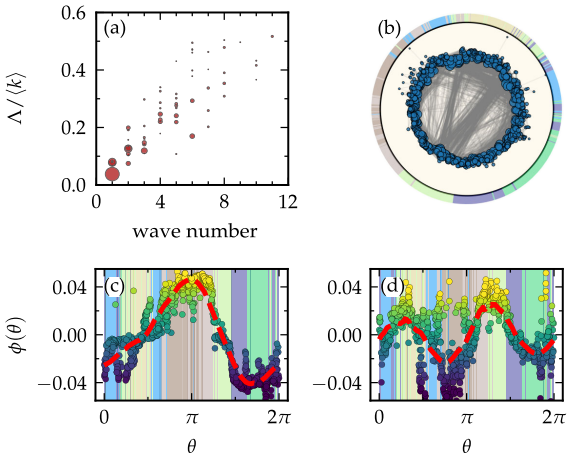

FIG. 9. Analysis of a human connectome network [84]. (a) Dispersion relation between the wave numbers of the dominant mode of the Laplacian eigenvectors and their rescaled eigenvalues. The size of the points is proportional to the height of the largest peak in the Fourier spectrum. (b) Hyperbolic representation of the network, where the node size is proportional to the hidden degree κ. The colored outer ring shows the partition in communities according to the Louvain algorithm [85]. (c),(d) The eigenvector with wave number one (c) and two (d) for which the pattern is most significant. The color follows $\phi(\theta)$ but rescaled such that the values lie between the 5th and 95th percentile of their original range. The background colors again represent the communities. The red dotted line represents the trend using the Savitzky-Golay filter with window size π.

network displays a modular or community organization, as revealed by a Louvain algorithm analysis, this alone cannot account for the observed patterns. Rather, geometry is responsible for this phenomenon.

VI. CONCLUSIONS

The small-world property present in complex networks suggests, *a priori*, that networks in the real world are infinite dimensional structures, so that geometry plays a marginal role. Yet, network geometry stands today as the most parsimonious and comprehensive description of this class of systems. However, beyond providing an explanation of the observed topological structure of real networks, it is not clear how network geometry influences the dynamics taking place on them. In this work, we show that geometric patterns may emerge in complex networks in a wide class of reaction-diffusion dynamics, as observed also in other types of dynamical processes such as opinion dynamics [86] and games [87]. Such patterns are already encoded in the structure of the Laplacian matrix as a result of the (hidden) metric structure of real networks. Interestingly, reaction-diffusion processes taking place on such networks are able to sense their geometric nature even when they show extreme disorder induced by heterogeneous degree distributions and a large fraction of long-range links making them small worlds.

In this work, we provide a theoretical framework to understand this phenomenon and to quantify the role that the different topological properties of networks have on the emerging patterns. This is done in the framework of undirected networks. Of course, real networks often contain directionality [88], and it has previously been shown that directed networks also support the Turing instability. In fact, the existence of directed links in a network has even been shown to amplify the region in parameter space where the homogeneous steady state is unstable, allowing for more easily accessible pattern formation. It is therefore important to expand the results we present in this paper to the directed geometric networks [89].

In addition to developing the theoretical tools for studying geometric patterns formation, significant insight is gained from the fact that Turing patterns can also be detected in real complex networks when the hidden similarity space is properly highlighted. This strongly suggests that there must exists a deep connection between networks' functions and the underlying geometry. Finding such yet unknown connection may shed light on one of the most fundamental questions in network science, namely, the connection between the topology and function of complex systems. This is particularly relevant in biological networks, where morphogenesis stands as a fundamental principle behind the organization of living systems.

ACKNOWLEDGMENTS

We acknowledge support from Grant No. PID2019–106290 GB-C22 funded by MCIN/AEI/10.13039/501100011033, and Generalitat de Catalunya Grant No. 2021SGR00856. M. B. acknowledges the ICREA Academia award, funded by the Generalitat de Catalunya. J. v d K. acknowledges support from the Ministry of Universities of Spain in the form of the FPU predoctoral contract.

APPENDIX

1. Diffusion dynamics on graphs

Let us focus on the diffusion of a single species on a simple undirected and globally connected network with adjacency matrix $\mathbb{A} \equiv \{a_{ij}\}$, $i, j = 1, \ldots, N$, and let $n_i(t)$ be the number of particles at node i at time t. We assume particles do not interact with each other and that nodes can accumulate an arbitrary number of particles on them. Once at node i, a particle jumps away from it at constant rate ζ_i. That is, each particle defines a continuous-time random walk [90,91] with dwell time probability density $\psi_i(\tau) = \zeta_i e^{-\zeta_i \tau}$. When a particle jumps from node i, it chooses one of i's neighbors at random. We can write the following equation for the stochastic evolution of $n_i(t)$ from t to $t + dt$:

$$n_i(t+dt) = n_i(t) + \sum_{j=1}^{N} \frac{a_{ij}}{k_j} \sum_{l=1}^{n_j(t)} \eta_j^l(t, dt) - \sum_{l=1}^{n_i(t)} \eta_i^l(t, dt), \tag{A1}$$

where $\eta_j^l(t, dt)$ is a random variable controlling the event that one of the $n_j(t)$ particles sitting at node j jumps to a different node in the interval $(t, t + dt)$. That is, $\eta_j^l(t, dt) = 1$ with probability $\zeta_j dt$ and $\eta_j^l(t, dt) = 0$ otherwise. By taking first averages over the random variables η and then over $n(t)$, we obtain the equation for the average number of particles at node i, $\langle n_i(t) \rangle \equiv u_i(t)$:

$$\frac{du_i(t)}{dt} = \sum_{j=1}^{N} \zeta_j \left(\frac{a_{ij}}{k_j} - \delta_{ij} \right) u_j(t) = -\sum_{j=1}^{N} \frac{\zeta_j}{k_j} L_{ij} u_j(t), \tag{A2}$$

where L_{ij} is the Laplacian matrix [50],

$$L_{ij} = k_j \delta_{ij} - a_{ij}. \tag{A3}$$

The steady state solution of Eq. (A2) is given by the eigenvector of zero eigenvalue of the Laplacian matrix. This implies that

$$\frac{\zeta_i u_i^{\mathrm{st}}}{k_i} = \text{const.} \tag{A4}$$

Therefore, if particles diffuse at the same rate in all nodes—so with $\zeta_i = \zeta,\ \forall\ i$—then the average concentration at node i is proportional to k_i and only when $\zeta_i \propto k_i$ the average concentration of particles is the same everywhere. We then make the choice $\zeta_i = \epsilon k_i$ and the diffusion equation finally reads

$$\frac{du_i(t)}{dt} = -\epsilon \sum_{j=1}^{N} L_{ij} u_j(t). \tag{A5}$$

Similarly to the case of diffusion in continuous media, we call ϵ the diffusion coefficient of the species in the network, even though, unlike diffusion in the continuum, it has dimensions of inverse of time.

2. Dispersion relation

To compute the dispersion relation in quenched networks, we generate a large number of them from the $\mathbb{S}^1/\mathbb{H}^2$ model for a given set of parameters β, γ, and $\langle k \rangle$. For each such network, we compute its eigenvectors and eigenvalues sorted in increasing order. We then compute the discrete Fourier transform of the eigenvectors and measure the characteristic frequency as the one corresponding to the highest peak in the Fourier spectrum. To asses whether a peak in the spectrum is statistically significant, we define a null model where the entries of the components of the eigenvector are independently drawn from a normal distribution $\mathcal{N}(\mu, \sigma^2)$ with $\mu = 0$ and $\sigma^2 = N^{-1}$. The first condition comes from Eq. (6) and the second from the fact that eigenvectors are normalized. Denoting $\hat{\phi}_i^{\mathrm{rand}}$ as one of the N entries of the DFT of a random eigenvector from our null model, it can be shown that it satisfies the following distribution function:

$$\mathrm{Prob}(|\hat{\phi}_i^{\mathrm{rand}}|^2 < q) = 1 - e^{-q}. \tag{A6}$$

With this in hand, we can find the value q for which there is a probability p that at least one peak in the white noise Fourier spectrum lies above q. We choose a probability $p = 10^{-2}$ and take the corresponding value of q to be the minimal value a peak in the Fourier spectrum of one of the eigenvectors of a network generated by the model needs to cross to be considered periodic. Thus,

$$p = 1 - \prod_{i=1}^{N} \mathrm{Prob}(|\hat{\phi}_i|^2 < q), \tag{A7}$$

so that

$$q = -\ln[1 - (1-p)^{1/N}]. \tag{A8}$$

For each network, we repeat this procedure for all its eigenvectors, leaving us with a set of pairs (Λ, ω_c) of statistically significant characteristic frequencies, from where we can derive the dispersion relation as an average over many network realizations.

3. Dynamics on the network

In this paper we use the Mimura-Murray model to perform numerical simulations. In particular, as in Ref. [11], we choose the parameters as $a = 35,\ b = 16,\ c = 9$, and $d = 2/5$, which gives the fixed point $(\bar{u}, \bar{v}) = (5, 10)$. In this case, the critical value of σ above which the Turing instability arises is $\sigma_c = 15.5071$. We then set the value to $\sigma = 15.6$, slightly above the critical point. Unstable eigenvalues will then lie within the interval $[\Lambda_-, \Lambda_+]$ with

$$\Lambda_- = \frac{1.410\,26}{\epsilon} \quad \text{and} \quad \Lambda_+ = \frac{1.666\,67}{\epsilon}, \tag{A9}$$

and the most unstable one given by

$$\Lambda_{\max} = \frac{1.533\,25}{\epsilon}. \tag{A10}$$

To select a given eigenvalue of interest Λ^*, we set it to $\Lambda^* = \Lambda_{\max}$ and use Eq. (A10) to fix the value of ϵ. With all the parameters of the dynamics fixed, we set every node's initial condition to be the stationary one, that is, $(u_i(0), v_i(0)) = (\bar{u}, \bar{v})$ for all i except for a randomly chosen one, j, for which $(u_j(0), v_j(0)) = (\bar{u} + \delta, \bar{v} + \delta)$, where $\delta = 10^{-5}$ is a small perturbation. We then let the system evolve toward its steady state.

4. Cheeger constant for the $\mathbb{S}^1/\mathbb{H}^2$ model

It is worth mentioning an interesting property of the $\mathbb{S}^1/\mathbb{H}^2$ model concerning its spectral gap, defined as the smallest non-null eigenvalue of the Laplacian Λ_2. Given a graph generated by the $\mathbb{S}^1$ model, $\mathcal{G}_{\mathbb{S}^1}$, Cheeger's inequalities state that

$$\frac{[h(\mathcal{G}_{\mathbb{S}^1})]^2}{2k_c} \leq \Lambda_2 < 2h(\mathcal{G}_{\mathbb{S}^1}), \tag{A11}$$

where $h(\mathcal{G}_{\mathbb{S}^1})$ is the isoperimetric (or Cheeger) constant of the graph [71,72]. This constant defines the optimal cut of the graph in two disjoint sets of nodes. For any partition A and B in two disjoint sets of sizes N_A and N_B, the Cheeger constant is defined as the ratio between the number of edges connecting the two sets E_{AB} and the size of the smallest set, minimized over all possible bipartitions of the graph; that is,

$$h(\mathcal{G}_{\mathbb{S}^1}) = \min_A \left\{ \frac{E_{AB}}{\min(N_A, N_B)} \right\}. \tag{A12}$$

While computing the Cheeger constant is, in general, not possible, in the $\mathbb{S}^1/\mathbb{H}^2$ model we can calculate its scaling behavior with the system size as follows. Assuming that the optimal cut minimizing the Cheeger constant is made by splitting the unit circle in two continuous regions, in the case of the $\mathbb{S}^1$ model Eq. (A12) can be written as follows:

$$h(\mathcal{G}_{\mathbb{S}^1}) = \min_x \left[\frac{2\pi}{xN} \int_0^x \int_x^{2\pi} \left(\frac{N}{2\pi} \right)^2 \frac{d\theta_2 d\theta_1}{1 + (\frac{N\Delta\theta_{12}}{2\pi\hat{\mu}\langle k\rangle^2})^\beta} \right], \tag{A13}$$

where $\Delta\theta_{12} = \pi - |\pi - |\theta_1 - \theta_2||$. Here we define the two disjoint regions as $A = \{i | 0 < \theta_i < x\}$ and $B = \{i | x < \theta_i < 2\pi\} = \mathcal{G}_{\mathbb{S}^1} \backslash A$. As we have chosen $0 < x < \pi$, in the model the least amount of nodes reside in A and thus $\min(N_A, N_B) = N_A = xN/(2\pi)$, as shown in Eq. (A13). The second part of this equation represents the amount of links between regions A and B, i.e., E_{AB}. It can be shown that Eq. (A13) can be written as

$$h(\mathcal{G}_{\mathbb{S}^1}) = \min_x \left[\frac{1}{x} \frac{N}{\pi} \int_0^x \int_\theta^\pi \frac{d\theta d\Delta}{1 + \left(\frac{N\Delta}{2\pi\hat{\mu}\langle k\rangle^2} \right)^\beta} \right], \tag{A14}$$

which in turn can be solved exactly, giving

$$h(\mathcal{G}_{\mathbb{S}^1}) = \min_x \left[\frac{N}{2\pi} f(N, x) \right], \tag{A15}$$

where

$$\begin{aligned} f(N,x) = {} & 2\pi {}_2F_1 \left[\begin{matrix} 1, \frac{1}{\beta} \\ 1 + \frac{1}{\beta} \end{matrix} ; -\left(\frac{N}{2\hat{\mu}\langle k\rangle} \right)^\beta \right] \\ & + x \left(-2 {}_2F_1 \left[\begin{matrix} 1, \frac{1}{\beta} \\ 1 + \frac{1}{\beta} \end{matrix} ; -\left(\frac{Nx}{2\pi\hat{\mu}\langle k\rangle} \right)^\beta \right] \right. \\ & \left. + {}_2F_1 \left[\begin{matrix} 1, \frac{2}{\beta} \\ 1 + \frac{2}{\beta} \end{matrix} ; -\left(\frac{Nx}{2\pi\hat{\mu}\langle k\rangle} \right)^\beta \right] \right). \end{aligned} \tag{A16}$$

Here, ${}_2F_1\left[\begin{smallmatrix} a,b \\ c \end{smallmatrix} ; z \right]$ is the ordinary hypergeometric function. Note that we use a slightly different form than the standard ${}_2F_1[a, b; c; z]$ for aesthetic purposes. It can be shown that this scales as $h(\mathcal{G}_{\mathbb{S}^1}) \simeq c_1 N^{1-\beta} + c_2 N^{-1}$, irrespective of the choice of x. Since $\beta > 1$, this scaling relation implies that $h(\mathcal{G}_{\mathbb{S}^1})$ approaches zero in the thermodynamic limit and so does the spectral gap. This implies that for very large networks we expect to find eigenvalues arbitrarily close to zero. This is important because small eigenvalues are the ones with more visible and clear patterns. This derivation is valid only in the case of a homogeneous hidden degree distribution. However, numerical analysis indicates that the Cheeger constant decays to zero in the case of a heterogeneous distribution as well.

5. Real network properties

In this section we elaborate on the properties of the real networks considered in this paper as well as in the Supplemental Material [82].

(i) Airports, Ref. [92]: The data for the network were obtained from the Preferred RSocio-Commes Database of the National Flight Data Center (NFDC), part of the U.S. Federal Aviation Administration. Nodes represent airports or service centers and edges are created from strings of preferred routes recommended by the NFDC. The original network was directed.

(ii) CElegans-C, Refs. [93,94]: The nervous system network of the nematode *Caenorhabditis elegans*. Here, the nodes are the neurons and the edges represent the connections, specifically gap junctions and chemical synapses, between them. The original network was directed.

(iii) CElegans-G, Ref. [95]: A genetic interaction network for the nematode *C. elegans* where the nodes represent genes and the links interactions on the genetic level.

(iv) Commodities, Ref. [96]: A network where the nodes represent industrial sectors and the links the flows of goods and services between them. The data used are from 2007 and were prepared by the U.S. Bureau of Economic Analysis. The original network was directed.

(v) FriendsOFF, Ref. [97]: An off-line friendship network among students, created from a survey where each student was asked to list five male and five female friends. The nodes are in this case the students and the edges represent these friendship relations. The original network was directed.

(vi) Human-C, Ref. [84]: A connectome of the human brain where nodes represent small brain regions and the edges represent fibers connecting these regions based on white matter tractography, which is a method used to estimate axonal bundle trajectories. In this network both hemispheres are incorporated.

(vii) List contacts, Ref. [98]: A network generated from the daily dynamic contact networks collected during the Infectious SocioPatterns event that took place at the Science Gallery in Dublin, Ireland, during the art science exhibition Infections: Stay Away. Nodes represent individuals attending the gallery, and two nodes are connected if they interacted with each other during the visit.

TABLE I. Properties of the five real networks studied in Figs. 1 and 8. The parameter $\hat{r}$ gives the percentage of eigenvectors classified as periodic by the procedure described in Appendix A 2. The notation ** implies that the results are significant with $p = 0.01$.

Network	N	$\langle k \rangle$	β	γ	$\hat{r}$
Airports	1226	3.9	1.0	4	7.1%**
CElegans-C	279	16.4	1.5	3.3	3.2%**
CElegans-G	878	7.2	2.6	2.7	5.9%**
Commodities	374	5.8	1.1	2.8	2.4%**
FriendsOFF	2539	8.2	1.3	9	4.4%**
Human-C	989	36.1	2.3	8	7.5%**
List contacts	410	13.5	2.2	7.5	6.1%**
Malaria-G	307	18.3	2.9	9	3.9%**
Mouse-C	213	27.9	2.0	3.5	2.3%**
Power	4941	2.7	1.3	10	11.0%**
URV-Email	1133	9.6	1.4	7	3.0%**
Wikipedia	4589	46.4	1.2	2.8	1.0%**
WTW 2013	189	5.8	1.9	2.4	5.8%**

(viii) Malaria-G, Ref. [99]: The network of recombinant antigen genes from the human malaria parasite *Plasmodium falciparum*, where nodes are var genes encoding for an antigen protein expressed on the surface of the infected red blood cell. These var genes are capable of interchanging bits of genetic information, thus creating a vast amount of slightly different genes that in turn create highly varying antigens that are hard for the human immune system to detect. Two nodes are connected if they share a substring of nucleotides of significant length, indicating that an interchange of genetic material between the two nodes has taken place.

(ix) Mouse-C, Ref. [100]: A connectome of the mouse brain where nodes represent anatomical subregions of the brain and the edges the physical connections between them. The original network was directed.

(x) Power, Ref. [101]: A network which represents the power grid of the western U.S. Here, nodes are transforms or power relay points and edges represent power lines running between these locations.

(xi) URV-Email, Ref. [102]: A network representing the exchange of emails between members of the Rovira i Virgili University in Spain, in 2003. The nodes represent the members and the edges the email traffic between them. The original version of the network was directed.

(xii) Wikipedia, Refs. [103,104]: A network where nodes represent Wikipedia articles and where two nodes are connected if there is a link between them. The original network was directed.

(xiii) WTW-2013, Refs. [105–107]: The world trade web as of 2013, where nodes represent countries and edges trade relations.

Table I shows the network properties of these networks.

[1] A. M. Turing, *The Chemical Basis of Morphogenesis*, Phil. Trans. R. Soc. B **237**, 37 (1952).

[2] A. Gierer and H. Meinhardt, *A Theory of Biological Pattern Formation*, Kybernetik **12**, 30 (1972).

[3] H. Meinhardt, *Models of Biological Pattern Formation* (Academic Press, New York, 1982), 10.1016/S0070-2153(07)81001-5.

[4] M. C. Cross and P. C. Hohenberg, *Pattern Formation Outside of Equilibrium*, Rev. Mod. Phys. **65**, 851 (1993).

[5] A. Koch and H. Meinhardt, *Biological Pattern Formation: From Basic Mechanisms to Complex Structures*, Rev. Mod. Phys. **66**, 1481 (1994).

[6] A. M. Zhabotinsky, M. Dolnik, and I. R. Epstein, *Pattern Formation Arising from Wave Instability in a Simple Reaction-Diffusion System*, J. Chem. Phys. **103**, 10306 (1995).

[7] M. Cross and H. Greenside, *Pattern Formation and Dynamics in Nonequilibrium Systems* (Cambridge University Press, Cambridge, England, 2009).

[8] S. Kondo and T. Miura, *Reaction-Diffusion Model as a Framework for Understanding Biological Pattern Formation*, Science **329**, 1616 (2010).

[9] D. Walgraef, *Spatio-Temporal Pattern Formation: With Examples from Physics, Chemistry, and Materials Science* (Springer Science & Business Media, New York, 2012).

[10] H. Othmer and L. Scriven, *Instability and Dynamic Pattern in Cellular Networks*, J. Theor. Biol. **32**, 507 (1971).

[11] H. Nakao and A. S. Mikhailov, *Turing Patterns in Network-Organized Activator–Inhibitor Systems*, Nat. Phys. **6**, 544 (2010).

[12] W. Horsthemke, K. Lam, and P. K. Moore, *Network Topology and Turing Instabilities in Small Arrays of Diffusively Coupled Reactors*, Phys. Lett. A **328**, 444 (2004).

[13] P. K. Moore and W. Horsthemke, *Localized Patterns in Homogeneous Networks of Diffusively Coupled Reactors*, Physica (Amsterdam) **206D**, 121 (2005).

[14] M. Asllani, J. D. Challenger, F. S. Pavone, L. Sacconi, and D. Fanelli, *The Theory of Pattern Formation on Directed Networks*, Nat. Commun. **5**, 4517 (2014).

[15] R. Muolo, M. Asllani, D. Fanelli, P. K. Maini, and T. Carletti, *Patterns of Non-normality in Networked Systems*, J. Theor. Biol. **480**, 81 (2019).

[16] J. Petit, B. Lauwens, D. Fanelli, and T. Carletti, *Theory of Turing Patterns on Time Varying Networks*, Phys. Rev. Lett. **119**, 148301 (2017).

[17] R. A. V. Gorder, *A Theory of Pattern Formation for Reaction-Diffusion Systems on Temporal Networks*, Proc. R. Soc. A **477**, 20200753 (2021).10.1098/rspa.2020.0753

[18] R. Muolo, L. Gallo, V. Latora, M. Frasca, and T. Carletti, *Turing Patterns in Systems with High-Order Interactions*, Chaos Solitons Fractals **166**, 112912 (2023).

[19] S. Gao, L. Chang, M. Perc, and Z. Wang, *Turing Patterns in Simplicial Complexes*, Phys. Rev. E **107**, 014216 (2023).

[20] M. Asllani, D. M. Busiello, T. Carletti, D. Fanelli, and G. Planchon, *Turing Patterns in Multiplex Networks*, Phys. Rev. E **90**, 042814 (2014).

[21] M. Asllani, D. M. Busiello, T. Carletti, D. Fanelli, and G. Planchon, *Turing Instabilities on Cartesian Product Networks*, Sci. Rep. **5**, 12927 (2015).

[22] N. E. Kouvaris, S. Hata, and A. Díaz-Guilera, *Pattern Formation in Multiplex Networks*, Sci. Rep. **5**, 10840 (2015).

[23] D. M. Busiello, T. Carletti, and D. Fanelli, *Homogeneous-per-Layer Patterns in Multiplex Networks*, Europhys. Lett. **121**, 48006 (2018).

[24] B. A. Siebert, C. L. Hall, J. P. Gleeson, and M. Asllani, *Role of Modularity in Self-Organization Dynamics in Biological Networks*, Phys. Rev. E **102**, 052306 (2020).

[25] M. Asllani, T. Carletti, and D. Fanelli, *Tune the Topology to Create or Destroy Patterns*, Eur. Phys. J. B **89**, 260 (2016).

[26] G. Cencetti, F. Battiston, T. Carletti, and D. Fanelli, *Generalized Patterns from Local and Non Local Reactions*, Chaos Solitons Fractals **134**, 109707 (2020).

[27] M.-T. Hütt, D. Armbruster, and A. Lesne, *Predictable Topological Sensitivity of Turing Patterns on Graphs*, Phys. Rev. E **105**, 014304 (2022).

[28] M. Boguñá, I. Bonamassa, M. D. Domenico, S. Havlin, D. Krioukov, and M. Á. Serrano, *Network Geometry*, Nat. Rev. Phys. **3**, 114 (2021).

[29] M. Á. Serrano, D. Krioukov, and M. Boguñá, *Self-Similarity of Complex Networks and Hidden Metric Spaces*, Phys. Rev. Lett. **100**, 078701 (2008).

[30] D. Krioukov, F. Papadopoulos, M. Kitsak, A. Vahdat, and M. Boguñá, *Hyperbolic Geometry of Complex Networks*, Phys. Rev. E **82**, 036106 (2010).

[31] L. Gugelmann, K. Panagiotou, and U. Peter, *Random Hyperbolic Graphs: Degree Sequence and Clustering*, in *Automata, Languages, and Programming. ICALP 2012*, edited by A. Czumaj, K. Mehlhorn, A. Pitts, and R. Wattenhofer, *Lecture Notes in Computer Science* Vol. 7392 (Springer, Berlin, Heidelberg, 2012), 10.1007/978-3-642-31585-5_51.

[32] E. Candellero and N. Fountoulakis, *Clustering and the Hyperbolic Geometry of Complex Networks*, Internet Math. **12**, 2 (2016).

[33] N. Fountoulakis, P. van der Hoorn, T. Müller, and M. Schepers, *Clustering in a Hyperbolic Model of Complex Networks*, Electron. J. Pro **26**, 1 (2021).

[34] J. van der Kolk, M. Á. Serrano, and M. Boguñá, *An Anomalous Topological Phase Transition in Spatial Random Graphs*, Commun. Phys. **5**, 245 (2022).

[35] M. A. Abdullah, N. Fountoulakis, and M. Bode, *Typical Distances in a Geometric Model for Complex Networks*, Internet Math. **1** (2017).10.24166/im.13.2017

[36] T. Friedrich and A. Krohmer, *On the Diameter of Hyperbolic Random Graphs*, SIAM J. Discrete Math. **32**, 1314 (2018).

[37] T. Müller and M. Staps, *The Diameter of KPKVB Random Graphs*, Adv. Appl. Probab. **51**, 358 (2019).

[38] M. Á. Serrano, D. Krioukov, and M. Boguñá, *Percolation in Self-Similar Networks*, Phys. Rev. Lett. **106**, 048701 (2011).

[39] N. Fountoulakis and T. Müller, *Law of Large Numbers for the Largest Component in a Hyperbolic Model of Complex Networks*, Ann. Appl. Probab. **28**, 607 (2018).

[40] M. Kiwi and D. Mitsche, *Spectral Gap of Random Hyperbolic Graphs and Related Parameters*, Ann. Appl. Probab. **28**, 941 (2018).

[41] G. García-Pérez, M. Boguñá, and M. Á. Serrano, *Multiscale Unfolding of Real Networks by Geometric Renormalization*, Nat. Phys. **14**, 583 (2018).

[42] M. Zheng, G. García-Pérez, M. Boguñá, and M. Á. Serrano, *Scaling Up Real Networks by Geometric Branching Growth*, Proc. Natl. Acad. Sci. U.S.A. **118**, e2018994118 (2021).

[43] F. Papadopoulos, M. Kitsak, M. Á. Serrano, M. Boguñá, and D. Krioukov, *Popularity versus Similarity in Growing Networks*, Nature (London) **489**, 537 (2012).

[44] A. Allard, M. Á. Serrano, G. García-Pérez, and M. Boguñá, *The Geometric Nature of Weights in Real Complex Networks*, Nat. Commun. **8**, 14103 (2017).

[45] K.-K. Kleineberg, M. Boguñá, M. Á. Serrano, and F. Papadopoulos, *Hidden Geometric Correlations in Real Multiplex Networks*, Nat. Phys. **12**, 1076 (2016).

[46] K.-K. Kleineberg, L. Buzna, F. Papadopoulos, M. Boguñá, and M. Á. Serrano, *Geometric Correlations Mitigate the Extreme Vulnerability of Multiplex Networks against Targeted Attacks*, Phys. Rev. Lett. **118**, 218301 (2017).

[47] K. Zuev, M. Boguñá, G. Bianconi, and D. Krioukov, *Emergence of Soft Communities from Geometric Preferential Attachment*, Sci. Rep. **5**, 9421 (2015).

[48] G. García-Pérez, M. Á. Serrano, and M. Boguñá, *Soft Communities in Similarity Space*, J. Stat. Phys. **173**, 775 (2018).

[49] A. Muscoloni and C. V. Cannistraci, *A Nonuniform Popularity-Similarity Optimization (nPSO) Model to Efficiently Generate Realistic Complex Networks with Communities*, New. J. Phys. **20**, 052002 (2018).

[50] P. van Mieghem, *Graph Spectra for Complex Networks* (Cambridge University Press, Cambridge, England, 2010), 10.1017/CBO9780511921681.

[51] I. Prigogine and R. Lefever, *Symmetry Breaking Instabilities in Dissipative Systems. II*, J. Chem. Phys. **48**, 1695 (1968).

[52] V. Castets, E. Dulos, J. Boissonade, and P. De Kepper, *Experimental Evidence of a Sustained Standing Turing-Type Nonequilibrium Chemical Pattern*, Phys. Rev. Lett. **64**, 2953 (1990).

[53] Q. Ouyang and H. L. Swinney, *Transition from a Uniform State to Hexagonal and Striped Turing Patterns*, Nature (London) **352**, 610 (1991).

[54] M. P. Harris, S. Williamson, J. F. Fallon, H. Meinhardt, and R. O. Prum, *Molecular Evidence for an Activator–Inhibitor Mechanism in Development of Embryonic Feather Branching*, Proc. Natl. Acad. Sci. U.S.A. **102**, 11734 (2005).

[55] L. A. Segel and S. A. Levin, *Application of Nonlinear Stability Theory to the Study of the Effects of Diffusion on Predator-Prey Interactions*, AIP Conf. Proc. **27**, 123 (1976).

[56] M. Mimura and J. Murray, *On a Diffusive Prey-Predator Model which Exhibits Patchiness*, J. Theor. Biol. **75**, 249 (1978).

[57] J. L. Maron and S. Harrison, *Spatial Pattern Formation in an Insect Host-Parasitoid System*, Science **278**, 1619 (1997).

[58] J. P. Gibert and J. D. Yeakel, *Laplacian Matrices and Turing Bifurcations: Revisiting Levin 1974 and the Consequences of Spatial Structure and Movement for Ecological Dynamics*, Theor. Ecol. **12**, 265 (2019).

[59] A. K. Fahimipour, F. Zeng, M. Homer, A. Traulsen, S. A. Levin, and T. Gross, *Sharp Thresholds Limit the Benefit of Defector Avoidance in Cooperation on Networks*, Proc. Natl. Acad. Sci. U.S.A. **119**, e2120120119 (2022).

[60] A. Brechtel, P. Gramlich, D. Ritterskamp, B. Drossel, and T. Gross, *Master Stability Functions Reveal Diffusion-Driven Pattern Formation in Networks*, Phys. Rev. E **97**, 032307 (2018).

[61] E. A. Bender and E. R. Canfield, *The Asymptotic Number of Labeled Graphs with Given Degree Sequences*, J. Comb. Theory Ser. A **24**, 296 (1978).

[62] B. Bollobás, *A Probabilistic Proof of an Asymptotic Formula for the Number of Labelled Regular Graphs*, Eur. J. Combinatorics **1**, 311 (1980).

[63] M. Molloy and B. Reed, *A Critical Point for Random Graphs with a Given Degree Sequence*, Random Struct. Algorithms **6**, 161 (1995).

[64] M. Molloy and B. Reed, *The Size of the Giant Component of a Random Graph with a Given Degree Sequence*, Comb. Probab. Comput. **7**, 295 (1998).

[65] A.-L. Barabási and R. Albert, *Emergence of Scaling in Random Networks*, Science **286**, 509 (1999).

[66] M. A. Serrano and M. Boguñá, *The Shortest Path to Network Geometry: A Practical Guide to Basic Models and Applications*, *Elements in Structure and Dynamics of Complex Networks* (Cambridge University Press, Cambridge, England, 2022), 10.1017/9781108865791.

[67] M. Boguñá, D. Krioukov, P. Almagro, and M. Á. Serrano, *Small Worlds and Clustering in Spatial Networks*, Phys. Rev. Res. **2**, 023040 (2020).

[68] M. Boguñá, F. Papadopoulos, and D. Krioukov, *Sustaining the Internet with Hyperbolic Mapping*, Nat. Commun. **1**, 1 (2010).

[69] M. Á. Serrano, M. Boguñá, and F. Sagués, *Uncovering the Hidden Geometry Behind Metabolic Networks*, Mol. Biosyst. **8**, 843 (2012).

[70] P. Almagro, M. Boguñá, and M. Á. Serrano, *Detecting the Ultra Low Dimensionality of Real Networks*, Nat. Commun. **13**, 6096 (2022).

[71] G. Pólya and G. Szegö, *Isoperimetric Inequalities in Mathematical Physics (AM-27)* (Princeton University Press, Princeton, NJ, 1951), http://www.jstor.org/stable/j.ctt1b9rzzn.

[72] J. Cheeger, *A Lower Bound for the Smallest Eigenvalue of the Laplacian*, in *Problems in Analysis*, edited by R. C. Gunning (Princeton University Press, Princeton, NJ, 1969), pp. 195–199, 10.1515/9781400869312-013.

[73] B. Derrida and Y. Pomeau, *Random Networks of Automata: A Simple Annealed Approximation*, Europhys. Lett. **1**, 45 (1986).

[74] S.-i. Amari, N. Fujita, and S. Shinomoto, *Four Types of Learning Curves*, Neural Comput. **4**, 605 (1992).

[75] U. Bastolla and G. Parisi, *Closing Probabilities in the Kauffman Model: An Annealed Computation*, Physica (Amsterdam) **98D**, 1 (1996).

[76] B. Luque and R. V. Solé, *Phase Transitions in Random Networks: Simple Analytic Determination of Critical Points*, Phys. Rev. E **55**, 257 (1997).

[77] T. Rohlf and S. Bornholdt, *Criticality in Random Threshold Networks: Annealed Approximation and Beyond*, Physica (Amsterdam) **310A**, 245 (2002).

[78] D. Vilone and C. Castellano, *Solution of Voter Model Dynamics on Annealed Small-World Networks*, Phys. Rev. E **69**, 016109 (2004).

[79] M. Boguná, C. Castellano, and R. Pastor-Satorras, *Langevin Approach for the Dynamics of the Contact Process on Annealed Scale-Free Networks*, Phys. Rev. E **79**, 036110 (2009).

[80] B. Guerra and J. Gómez-Gardenes, *Annealed and Mean-Field Formulations of Disease Dynamics on Static and Adaptive Networks*, Phys. Rev. E **82**, 035101(R) (2010).

[81] S. C. Ferreira, R. S. Ferreira, and R. Pastor-Satorras, *Quasistationary Analysis of the Contact Process on Annealed Scale-Free Networks*, Phys. Rev. E **83**, 066113 (2011).

[82] See Supplemental Material at http://link.aps.org/supplemental/10.1103/PhysRevX.13.021038 for an analysis of the periodicity of the eigenvectors of several real networks.

[83] G. García-Pérez, A. Allard, M. Á. Serrano, and M. Boguñá, *Mercator: Uncovering Faithful Hyperbolic Embeddings of Complex Networks*, New J. Phys. **21**, 123033 (2019).

[84] P. Hagmann, L. Cammoun, X. Gigandet, R. Meuli, C. J. Honey, V. J. Wedeen, and O. Sporns, *Mapping the Structural Core of Human Cerebral Cortex*, PLoS Biol. **6**, e159 (2008).

[85] V. D. Blondel, J.-L. Guillaume, R. Lambiotte, and E. Lefebvre, *Fast Unfolding of Communities in Large Networks*, J. Stat. Mech. (2008) P10008.

[86] E. Ortiz and M. Á. Serrano, *Multiscale Voter Model on Real Networks*, Chaos Solitons Fractals **165**, 112847 (2022).

[87] K.-K. Kleineberg, *Metric Clusters in Evolutionary Games on Scale-Free Networks*, Nat. Commun. **8**, 1888 (2017).

[88] J. D. O'Brien, K. A. Oliveira, J. P. Gleeson, and M. Asllani, *Hierarchical Route to the Emergence of Leader Nodes in Real-World Networks*, Phys. Rev. Res. **3**, 023117 (2021).

[89] A. Allard, M. Ángeles Serrano, and M. Boguñá, *Geometric Description of Clustering in Directed Networks*, arXiv:2302.09055.

[90] E. W. Montroll and G. H. Weiss, *Random Walks on Lattices. II*, J. Math. Phys. **6**, 167 (1965).

[91] G. H. Weiss, *Aspects and Applications of the Random Walk* (North-Holland, Amsterdam, 1994), 10.1007/BF02179402.

[92] J. Kunegis, *KONECT: The Koblenz Network Collection*, in *Proceedings of the 22nd International Conference on World Wide Web (WWW '13 Companion)* (ACM, New York, 2013), pp. 1343–1350, 10.1145/2487788.2488173.

[93] Y.-Y. Ahn, H. Jeong, and B. J. Kim, *Wiring Cost in the Organization of a Biological Neuronal Network*, Physica (Amsterdam) **367A**, 531 (2006).

[94] J. S. Kim and M. Kaiser, *From Caenorhabditis elegans to the Human Connectome: A Specific Modular Organization Increases Metabolic, Functional and Developmental Efficiency*, Phil. Trans. R. Soc. B **369**, 20130529 (2014).

[95] A. Cho, J. Shin, S. Hwang, C. Kim, H. Shim, H. Kim, H. Kim, and I. Lee, *WormNet v3: A Network-Assisted Hypothesis-Generating Server for, Caenorhabditis elegans*, Nucleic Acids Res. **42**, W76 (2014).

[96] D. Grady, C. Thiemann, and D. Brockmann, *Robust Classification of Salient Links in Complex Networks*, Nat. Commun. **3**, 864 (2012).

[97] J. Moody, *Peer Influence Groups: Identifying Dense Clusters in Large Networks*, Soc. Networks **23**, 261 (2001).

[98] L. Isella, J. Stehlé, A. Barrat, C. Cattuto, J.-F. Pinton, and W. V. den Broeck, *What's in a Crowd? Analysis of Face-to-Face Behavioral Networks*, J. Theor. Biol. **271**, 166 (2011).

[99] D. B. Larremore, A. Clauset, and C. O. Buckee, *A Network Approach to Analyzing Highly Recombinant Malaria Parasite Genes*, PLoS Comput. Biol. **9**, e1003268 (2013).

[100] S. W. Oh *et al.*, *A Mesoscale Connectome of the Mouse Brain*, Nature (London) **508**, 207 (2014).

[101] D. J. Watts and S. H. Strogatz, *Collective Dynamics of 'Small-World' Networks*, Nature (London) **393**, 440 (1998).

[102] R. Guimerà, L. Danon, A. Díaz-Guilera, F. Giralt, and A. Arenas, *Self-Similar Community Structure in a Network of Human Interactions*, Phys. Rev. E **68**, 065103(R) (2003).

[103] R. West, J. Pineau, and D. Precup, *Wikispeedia: An Online Game for Inferring Semantic Distances between Concepts*, in *Proceedings of the International Joint Conference on Artificial Intelligence, California, 2009*.

[104] R. West and J. Leskovec, *Human Waynding in Information Networks*, in *Proceedings of the 21st International confErence on World Wide Web (WWW '12)* (ACM, 2012), pp. 619–628, 10.1145/2187836.2187920.

[105] M. Á. Serrano and M. Boguñá, *Topology of the World Trade Web*, Phys. Rev. E **68**, 015101(R) (2003).

[106] M. Á. Serrano, M. Boguñá, and A. Vespignani, *Patterns of Dominant Flows in the World Trade Web*, J. Econ. Interact. Coord. **2**, 111 (2007).

[107] G. García-Pérez, M. Boguñá, A. Allard, and M. A. Serrano, *The Hidden Hyperbolic Geometry of International Trade: World Trade Atlas 1870–2013*, Sci. Rep. **6**, 33441 (2016).